Geophysical Research Letters

RESEARCH LETTER
10.1029/2019GL084196

Improved Predictability of the Indian Ocean Dipole Using Seasonally Modulated ENSO Forcing Forecasts

Sen Zhao[1,2], Fei-Fei Jin[2], and Malte F. Stuecker[3,4]

[1]CIC-FEMD/ILCEC, Key Laboratory of Meteorological Disaster of Ministry of Education, and College of Atmospheric Science, Nanjing University of Information Science and Technology, Nanjing, China, [2]Department of Atmospheric Sciences, University of Hawai'i at Mānoa, Honolulu, HI, USA, [3]Center for Climate Physics, Institute for Basic Science, Busan, South Korea, [4]Pusan National University, Busan, South Korea

Key Points:
- A stochastic-dynamical model using seasonally modulated ENSO forcing has generally higher skill in predicting the IOD than CFSv2 and SINTEX
- Operational IOD predictability beyond persistence is mostly controlled by ENSO predictability and the signal-to-noise ratio of the system
- Potential future ENSO improvements in GCMs could directly translate to more skillful IOD predictions using the stochastic-dynamical model

Supporting Information:
- Supporting Information S1

Correspondence to:
F.-F. Jin and M. F. Stuecker,
jff@hawaii.edu;
stuecker@pusan.ac.kr

Citation:
Zhao, S., Jin, F.-F., & Stuecker, M. F. (2019). Improved predictability of the Indian Ocean Dipole using seasonally modulated ENSO forcing forecasts. *Geophysical Research Letters*, *46*. https://doi.org/10.1029/2019GL084196

Received 20 JUN 2019
Accepted 6 AUG 2019
Accepted article online 9 AUG 2019

Abstract Despite recent progress in seasonal forecast systems, the predictive skill for the Indian Ocean Dipole (IOD) remains typically limited to a lead time of one season or less in both dynamical and empirical models. Here we develop a simple stochastic-dynamical model (SDM) to predict the IOD using seasonally modulated El Niño–Southern Oscillation (ENSO) forcing together with a seasonally modulated Indian Ocean coupled ocean-atmosphere feedback. The SDM, with either observed or forecasted ENSO forcing, exhibits generally higher skill and longer lead times for predicting IOD events than the operational Climate Forecast System version 2 and the Scale Interaction Experiment–Frontier system. The improvements mainly originate from better prediction of ENSO-dependent IOD events and from reducing false alarms. These results affirm our hypothesis that operational IOD predictability beyond persistence is largely controlled by ENSO predictability and the signal-to-noise ratio of the system. Therefore, potential future ENSO improvements in models should translate to more skillful IOD predictions.

Plain Language Summary The Indian Ocean Dipole (IOD) is a prominent climate phenomenon occurring in the tropical Indian Ocean. Since IOD events have large socioeconomic and environmental impacts globally, predicting them has become a scientific challenge of considerable importance. The current predictive skill for the IOD exhibited by operational seasonal forecast models remains poor compared to that for the El Niño–Southern Oscillation (ENSO), partly due to the failure of models to realistically simulate the observed ENSO-IOD relationship. To this end, we have developed a simple stochastic-dynamical model (SDM) to predict the IOD using the observed IOD-ENSO relationship together with operational ENSO forecast information. The SDM demonstrates considerably improved IOD forecast skill compared to current operational models.

1. Introduction

The Indian Ocean Dipole (IOD) is a prominent coupled ocean-atmosphere mode of climate variability in the Indian Ocean (Saji et al., 1999; Webster et al., 1999), which shows a strong coupling with the seasonal cycle. IOD events tend to develop in boreal summer, peak during autumn (September–November (SON)), and decay rapidly in winter (Saji et al., 1999; Saji & Yamagata, 2003a). The positive phase of IOD events is characterized by negative sea surface temperature (SST) anomalies in the south-eastern equatorial Indian Ocean and positive SST anomalies in the western equatorial Indian Ocean. The latent heat release associated with the IOD is an important energy source driving Asian-Australian monsoon variability and global climate variability via atmospheric Rossby wave trains (Cai et al., 2011; Chan et al., 2008; Guan & Yamagata, 2003; Liu & Lu, 2007; Saji & Yamagata, 2003b; Yuan et al., 2008). Several studies have also argued that the IOD can influence either the simultaneous or following year El Niño–Southern Oscillation (ENSO) evolution (Izumo et al., 2010; Luo et al., 2010). Many severe climate events with pronounced societal and economic impacts can be attributed to the IOD. These include for instance haze problems in Indonesia associated with forest fires, droughts in Australia, and floods in East Africa (Cai et al., 2014; Luo et al., 2015). Therefore, skillful IOD predictions with a long enough lead time would potentially allow for the implementation of mitigation measures and thereby could provide pronounced societal benefits.

The predictability of Indian Ocean SST anomalies associated with the IOD is significantly smaller compared to those in the Pacific associated with ENSO (Luo et al., 2007; Luo et al., 2008; Shi et al., 2012; Song et al.,

2008; Wajsowicz, 2005, 2007; Zhao & Hendon, 2009; Zhu et al., 2015). It has been suggested that the skillful prediction of IOD events is typically limited to a lead time of about two to three months (approximately one season) in current coupled atmosphere-ocean models (Liu et al., 2017; Shi et al., 2012), with slightly higher skill seen only for some individual strong IOD events (Luo et al., 2008). The predictive skill of the IOD exhibits a strong seasonality with a predictability barrier during boreal winter-spring (Feng et al., 2014; Wajsowicz, 2007; Wang et al., 2009). Moreover, the IOD events that co-occur with ENSO events tend to be more predictable, while the remaining events appear to be initiated by weather noise and exhibit a lower predictability (Song et al., 2008; Zhao & Hendon, 2009). These results indicate that the failure of models to accurately simulate the observed IOD–ENSO relationship (discussed below) might be one reason that limits the predictive skill of the IOD in operational forecasts.

There has been a long-standing discussion in the literature concerning the physical nature of the IOD–ENSO relationship. Some studies argue that the IOD is in fact an intrinsic climatic mode that is largely independent from ENSO (Behera et al., 2006; Saji et al., 1999; Webster et al., 1999), while other studies emphasize that IOD events can be externally initiated by ENSO (Annamalai et al., 2003; Kajtar et al., 2017; Yang et al., 2015; Zhang et al., 2015). Some of this debate might be explained by the fact that many studies did not carefully consider the seasonal dependence of the correlation between IOD and ENSO (see discussion in Stuecker et al. (2017)). Additionally, some studies argue that the IOD may trigger or modulate the characteristics of ENSO events (Behera & Yamagata, 2003; Izumo et al., 2010; Luo et al., 2010). By using a partially coupled model experiment with decoupled SST over the tropical Pacific, some studies (Crétat et al., 2017; Fischer et al., 2005; Wang et al., 2019) showed that the IOD still exists without ENSO, but with weaker amplitude and reduced Bjerknes feedback in the Indian Ocean. Furthermore, several studies showed evidence that only about one third of IOD events occur independently of ENSO events (Loschnigg et al., 2003; Stuecker et al., 2017). Recently, Stuecker et al. (2017) developed a null hypothesis framework for the IOD similar to earlier ideas presented in Dommenget and Jansen (2009) and showed that most of the IOD variability can be explained by deterministic interactions between the annual cycle and ENSO (via the ENSO Combination Mode: C-mode; Stuecker et al., 2013, 2015). Given that ENSO is more predictable than the IOD and exhibits longer skillful lead times in current operational models (Barnston et al., 2012), we should expect an improvement of IOD predictive skill when utilizing the observed statistical relationship between ENSO and the IOD in combination with operational ENSO forecasts. Here we show using a relatively simple model framework that an improved hindcast skill of the IOD dipole mode index (DMI) can be achieved in comparison to coupled general circulation model ensemble forecasts of the IOD.

2. Data and Methods

2.1. Data

We utilize the retrospective and real-time nine-month 24-member ensemble SST forecasts from the National Centers for Environment Prediction Climate Forecast System version 2 (CFSv2; Saha et al., 2014) for the periods of January 1982–March 2011 and April 2011–December 2015, respectively. The forecast SST anomalies are calculated with respect to the climatology from January 1982 to December 2015 at each lead time for each member. Our conclusions are not affected when we eliminate the discontinuous forecast biases by calculating the forecast anomalies using two different climatological periods of 1982–1998 and 1999–2015 (Barnston et al., 2017). As we will use the CFSv2 ENSO forecast as the forcing driving a simple model, here we only consider the multimember ensemble mean throughout this study. The SST observations used here are the NOAA Optimum Interpolation SST v2 (Reynolds et al., 2002). The observed SST anomalies are calculated with respect to the same climatology period of 1982–2015. The Niño-3.4 index is defined as the SST anomalies averaged over the region 120°W–170°W and 5°S–5°N. The DMI is defined as the area averaged SST anomalies in the western IO (50°E–70°E, 10°S–10°N) minus those in the eastern IO (90°E–110°E, 10°S–EQ; Saji et al., 1999).

2.2. A Stochastic-Dynamical Model for the DMI

Previous studies have developed a DMI regression model with a discrete representation of the temperature tendency equation (Dommenget & Jansen, 2009; Shi et al., 2012). In contrast, here we treat the IOD as a

continuous dynamical system driven by both ENSO forcing and stochastic forcing. We use a physically motivated stochastic-dynamical model (SDM) for the IOD, similar to Stuecker et al. (2017):

$$\frac{dT}{dt} = -\lambda(t)T(t) + \alpha(t)T_{\mathrm{ENSO}}(t) + \sigma_0\xi(t), \tag{1}$$

where T is the monthly DMI, $T_{\mathrm{ENSO}}(t)$ is the monthly Niño-3.4 index, $\lambda(t)$ is the damping rate of T, $\alpha(t)$ is the ENSO forcing strength, $\xi(t)$ is the stochastic forcing, and σ_0 is the magnitude of stochastic forcing. The first term on the right-hand side represents seasonally modulated damping that arises from the net effect of coupled air-sea Indian Ocean feedback, including contributions from the positive Bjerknes feedback (Annamalai et al., 2003; Hong et al., 2008; Saji et al., 2006; Zhang et al., 2015) and the negative SST-cloud-radiation feedback (Cai & Qiu, 2013; Li et al., 2003; Ng et al., 2014). The second term on the right-hand side represents the ENSO forcing, which includes both the direct ENSO effect and its interaction with the annual cycle (via the aforementioned C-mode). At the leading order, the seasonality of $\lambda(t)$ and $\alpha(t)$ are approximated as the annual harmonic function of $\lambda_0[1+D\cos(\omega t+\varphi_D)]$ and $\alpha(t) = \alpha_0[1+A\cos(\omega t+\varphi_A)]$, respectively, where $\omega = \pi/(6\ \mathrm{months})$. The stochastic forcing term is important for the initiation of ENSO-independent IOD events and also may contain deterministic high-frequency variability. Following the same approach as Jin et al. (2007), we use simple red noise to force the SDM,

$$\frac{d\xi}{dt} = -m\xi(t) + w(t), \tag{2}$$

where $w(t)$ denotes white noise with a Gaussian distribution and the decorrelation time scale parameter m is set to 0.5 month in this study. We emphasize that the SDM without ENSO forcing is the original stochastic climate model (Frankignoul & Hasselmann, 1977; Hasselmann, 1976) with seasonally varying damping (De Elvira & Lemke, 1982).

The model parameters λ_0,D, φ_D, α_0, A, φ_A, and σ_0 can be estimated via multivariate linear regression using the observed DMI and Niño-3.4 indices (see Text S1, Table S1, and Figure S1 in the supporting information). The estimated growth rate and coupling strength are consistent with realistic damping values and C-mode forcing discussed in previous studies (Annamalai et al., 2003; Moon & Wettlaufer, 2017; Stuecker et al., 2013, 2015; Xie & Zhou, 2017). Furthermore, the observed IOD statistics are well reproduced in the reconstruction of the DMI using the SDM (see details in Text S2 and Figures S2–S4 in the supporting information). This SDM provides an opportunity to improve the predictability of IOD events by utilizing the observed statistical ENSO-IOD relationship. As we will compare the SDM to operational ensemble mean forecasts, the stochastic forcing term will be neglected in the remaining manuscript and the IOD treated as a purely deterministic process. Nevertheless, this stochastic forcing is important to explain ENSO-independent IOD events and the amplitude of IOD events in general. Thus, we hypothesize that identifying spatial noise patterns that are effective in initiating ENSO-independent IOD events might further improve future IOD predictions.

2.3. Cross-Validated Hindcast Experiments With the SDM

We conducted six experiments using the SDM with retrospective nine months forecasts for the period of January 1982–December 2015 (see Table S2 in the supporting information). In the first three experiments, we integrated the SDM initialized from the monthly observed (perfect) DMI conditions with the forcing applied in three different ways: (i) prescribing zero forcing, (ii) utilizing the observed (perfect) ENSO time evolution as the forcing, and (iii) using the ensemble mean of the CFSv2 ENSO forecast as the forcing. Accordingly, these experiments are referred to as SDM-Z, SDM-P, and SDM-F, respectively. By definition, the perfect DMI initial conditions result in a perfect skill at zero-month lead time in these experiments. However, the predicted SSTs in operational forecasts are always imperfect at zero-month lead time regardless of the SST prediction method. Therefore, to compare the predictive skill more fairly with CFSv2, we perform another three experiments with the same three types of forcing but initialized from the forecasted DMI derived from the CFSv2 ensemble mean forecasts at zero-month lead time, referred to as SDM-Z-F, SDM-P-F, and SDM-F-F, respectively. This explains the imperfect skill at zero-month lead time for the SDM-Z-F, SDM-P-F, SDM-F-F, and CFSv2 forecasts.

To compare the SDM performance with the coupled general circulation model results we used a simple cross-validation method. We split the whole data into two periods of 1982–1998 and 1999–2015 (by the middle of the data period), and estimated all model parameters for each period (resulting in two different training periods). Then we forecasted the DMI for the respective other period (two validation periods). We show the results in Figures 1–3 and S5–S10 based on the cross-validated hindcasts which are the forecasts only from the above validation periods. Additionally, our conclusions remain robust if we split the whole data at a different point, for example, 1996/1997, 1997/1998, or 2000/2001 (not shown).

2.4. Predictive Skill Assessment

The predictive skill of the IOD is quantified in terms of the anomaly correlation coefficient (ACC) and root-mean-square errors (RMSE). To assess seasonal performance, the RMSE is normalized by the standard deviation of the observation for each season individually (NRMSE) to allow for fair comparison with previous studies (e.g., Doi et al., 2017). Skills are calculated based on time series of running three-month means for both the observations and model hindcasts at each lead time (details in Text S3 in the supporting information), in order to remove the intraseasonal noise and to be consistent with typical seasonal forecast product skill evaluation (Luo et al., 2007; Shi et al., 2012). Our conclusions are not affected by the running mean, although the predictive skill estimate is more conservative using nonsmoothed monthly data in comparison with the skill assessment of running three-month means. The one-sided test of the Fisher z-transformation was used to test statistical significance of the ACC differences.

3. Results

3.1. Prediction Skill for the IOD

As a measure of overall predictive skill of the seasonal DMI, Figures 1a and 1b show the ACC and RMSE metrics between the observed and predicted DMI as function of lead month for the individual models (the aforementioned six cross-validated SDM experiments, persistence forecast, and the dynamical CFSv2 DMI forecast) for the 1982–2015 period. We observe a decrease of predictive skill, characterized by a decline of the ACC and incline of the RMSE, with increasing lead time for all models. The skills of both the persistence model (black curves in Figures 1a and 1b) and CFSv2 (blue curves in Figures 1a and 1b) decline rapidly, with ACC skill below 0.5 beyond a three-month lead time, which is consistent with previous studies (Shi et al., 2012; Zhu et al., 2015) that showed that CFSv2 does not have significantly better skill in predicting IOD events than a persistence forecast (see also Figure S5a). In contrast, it is evident that the SDM exhibits better predictive skill compared to the persistence forecast, as shown by the ACC and RMSE measures. The SDM results are not very sensitive to the DMI initial conditions with small ACC skill differences (values less than 0.1) only at very short lead times (approximately one to two months; Figure S5c). As expected, without any ENSO forcing (SDM-Z-F, orange dashed lines in Figures 1a and 1b), the SDM demonstrates very similar ACC skill to the persistence forecast at one- to six-month lead times (Figure S5a). Using the CFSv2 ENSO forecast as forcing (SDM-F-F, green dashed lines in Figures 1a and 1b), we see better predictive skills of the SDM compared to the persistence forecast with ACC differences of about 0.2 at approximately four- to six-month lead time (Figure S5a). Once we force the SDM with the actual observed ENSO forcing (SDM-P-F, red dashed lines in Figures 1a and 1b), we observe further predictive skill improvements for the DMI, especially at lead times longer than four months (Figure S5a). While being largely consistent, these results show improved skill compared to a discrete regression model based on a similar physical hypothesis (Dommenget & Jansen, 2009). We hypothesize that the SDM demonstrates improved skill over this discrete regression model probably because the SDM has less free parameters for the representation of the observed growth rate and coupling strength.

The SDM also shows improved DMI predictive skill at approximately 2- to six-month lead time compared with CFSv2 (Figure S5b). The ACC of both SDM-P and SDM-P-F is above 0.6 at three-month lead time and stays above 0.5 at six months and longer lead times (Figure 1a). Similarly, the corresponding RMSE approaches ~0.35 at six months and longer lead times. If a skillful prediction of the IOD is defined by an ACC larger than 0.5, then the SDM-P-F experiment provides a skillful DMI hindcast at lead times of up to two seasons while CFSv2 only shows skill at one season lead time (the same as persistence). The reduced RMSE for SDM-P-F over CFSv2 is around 10–20% of the standard deviation of the observed DMI at four- to nine-month lead times. As ENSO forecasts exhibit predictive skill with up to several seasons lead time,

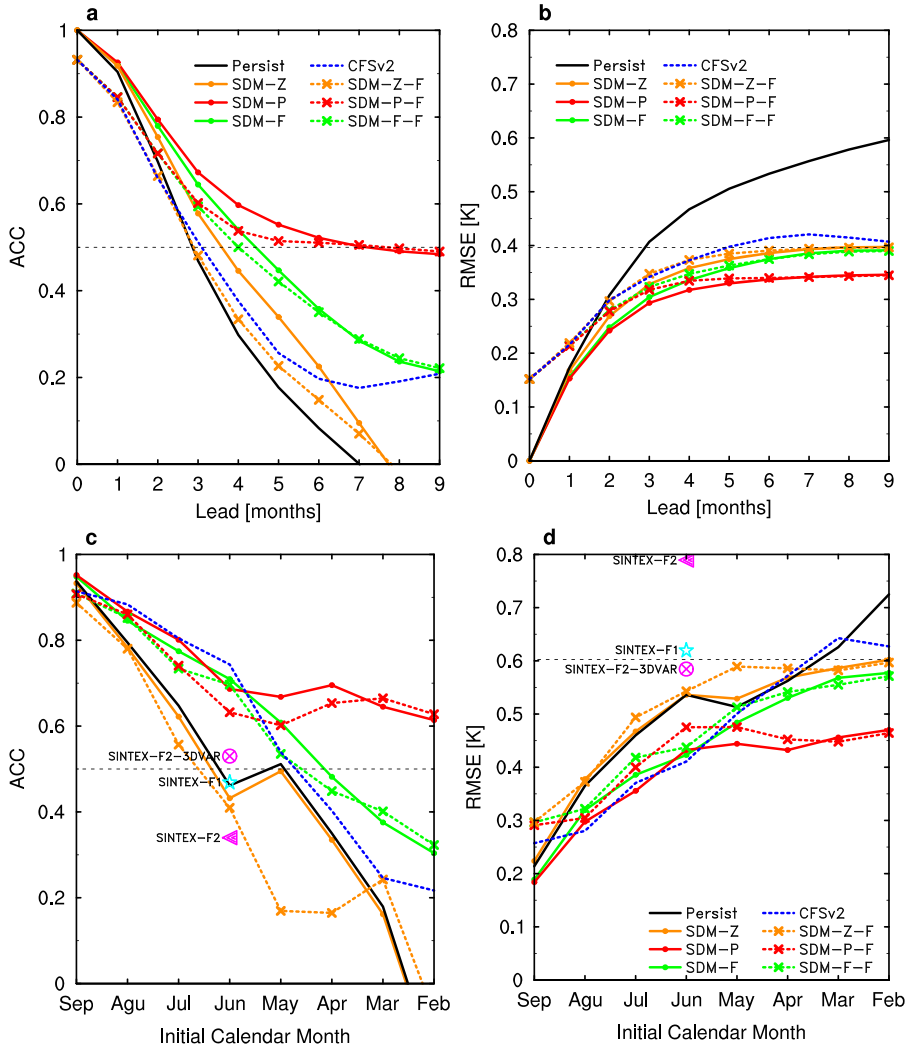

Figure 1. (a) Anomaly correlation coefficient (ACC) and (b) root-mean-square errors (RMSE) (unit: K) between observed and predicted DMI, as a function of lead time for the individual models: persistence (black solid), CFSv2 (blue dashed), cross-validated SDM-Z (orange solid), SDM-Z-F (orange dashed), SDM-P (red solid), SDM-P-F (red dashed), SDM-F (green solid), and SDM-F-F (green dashed). Both forecasts and verification were smoothed with a three-month running mean prior to computing ACC and RMSE. (c and d) The same as in (a) and (b), respectively, but for predictive skills of the DMI averaged for peak season SON as a function of initialization month in each year. The black dashed reference lines denote ACC of 0.5 (a and c) and RMSE of 0.4 (b, the standard deviation of the observed DMI) and 0.6 (d, the standard deviation of the observed DMI at SON), respectively. The skill metrics of the SINTEX systems for June initialization are shown in (c) and (d) by colored markers (adopted from Tables 2 and 3, respectively, in Doi et al. (2017) for the period of 1983–2015).

the SDM can translate this to IOD predictive skill that can be utilized in an operational setting. By using the ENSO hindcast information, SDM-F-F shows better cross-validated skill compared to CFSv2 with ACC differences well above 0.1 at approximately three- to six-month lead times (Figure S5b) and RMSE differences of around ~10% of the standard deviation of the observed DMI at five- to seven-month lead times (Figure S5e).

Figures 1c and 1d illustrate the ACC and RMSE metrics as a function of initialization month concentrating on the DMI averaged for boreal fall (SON), which is the IOD peak season. We find that the SDM with either observed (SDM-P-F) or forecasted ENSO forcing (SDM-F-F) has comparable but slightly weaker predictive skills of SON DMI to CFSv2 when the prediction is initialized later after May. However, when the prediction is initialized prior to May, the SDMs beat CFSv2 with a slightly better skill for SDM-F-F and pronounced improved skill for SDM-P-F in terms of both ACC and RMSE. The Scale Interaction Experiment–Frontier

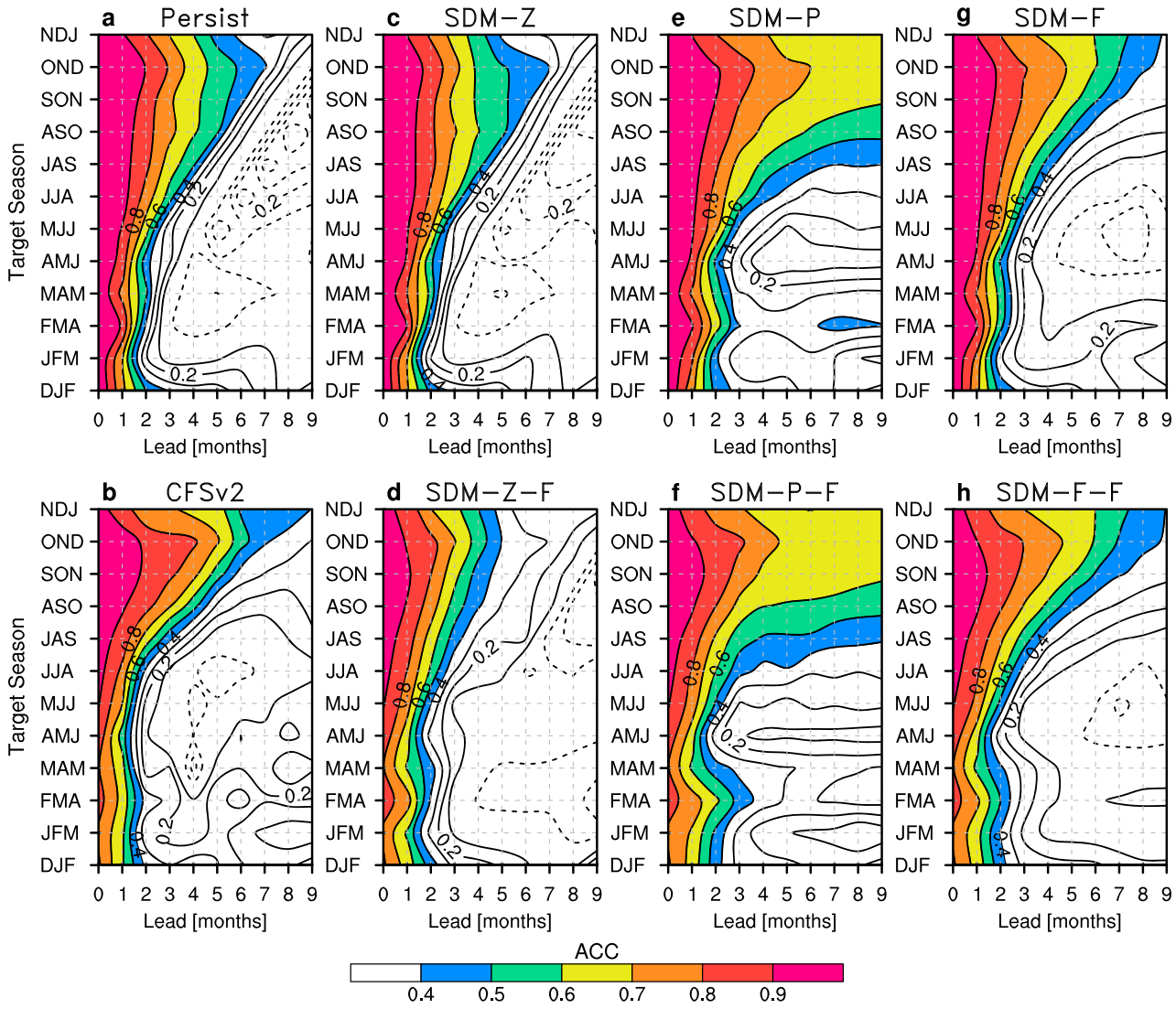

Figure 2. Seasonality of predictive skills of running three-month mean DMI for the different models (persistence, CFSv2, and cross-validated SDMs). Anomaly correlation coefficient (ACC) between model forecasts and observations as a function of lead time and target season. The contour interval is 0.1.

version 1 (SINTEX-F1) and version 2 (SINTEX-F2) prediction systems have successfully predicted several IOD events a few seasons ahead (Doi et al., 2016; Luo et al., 2007). By introducing a new three-dimensional variational ocean data assimilation (3DVAR) method in SINTEX-F2, SINTEX-F2-3DVAR demonstrated improved prediction skill compared to SINTEX-F2 (Doi et al., 2017). Both CFSv2 and the SDMs with ENSO forgings show much improved DMI prediction skill compared to the SINTEX-F1/F2/F2-3DVAR systems and the persistence forecast when the prediction is initialized in June. The difference in ACCs between SDM-F-F (ACC = 0.72) and SINTEX-F2-3DVAR (ACC = 0.53) is 0.19 (p = 0.11; one-sided test of the Fisher z transformation). This result demonstrates the superior skill of the SDM also when compared to the operational SINTEX-F prediction system. Together, these results strongly suggest that operational IOD predictability beyond persistence at lead times over one season is mostly determined by ENSO predictability and the signal-to-noise ratio in the system as hypothesized based on theory in Stuecker et al. (2017). While the SDMs exhibit considerable improvements in the IOD phase prediction (as captured by the ACC), they tend to underestimate the overall amplitude of the IOD (as captured by the RMSE). A possible explanation is that the intrinsic Indian Ocean processes as well as the stochastic forcing, which are not included in the present SDM hindcasts, may also contribute to the IOD event amplitude.

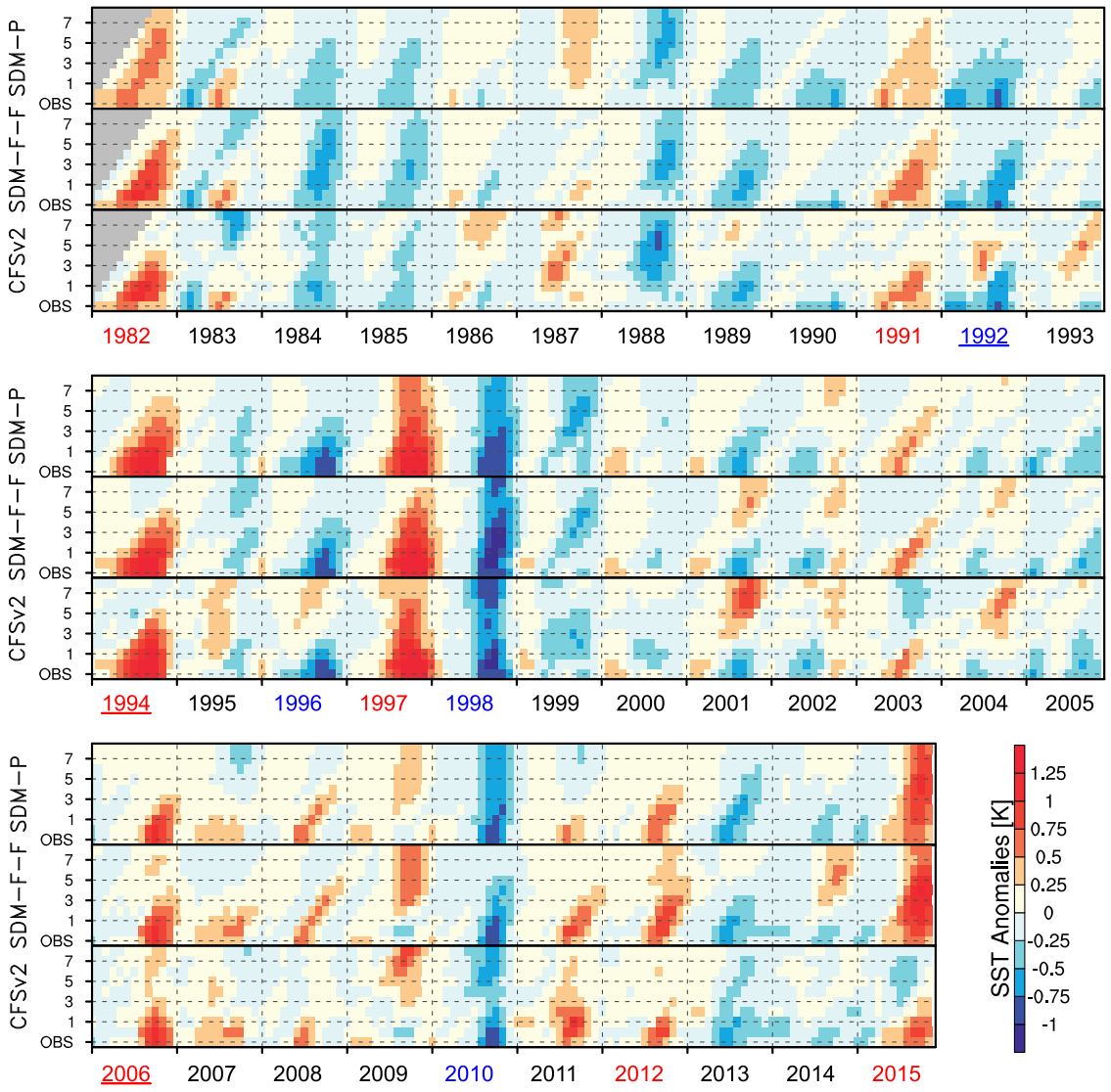

Figure 3. Predicted and observed DMI. Time series of running three-month mean DMI SST anomaly observations and the corresponding model predictions (cross-validated SDM-P, SDM-F-F, and CFSv2) for the same three-month period from start times ranging from zero- to eight-month leads. The bottom row shows the observations, while the nine rows above show the predictions at the nine increasing lead times (months). Observations range from January 1982 to December 2015. Strong positive and negative IOD years are marked with red and blue font separately and ENSO-independent IOD years are underlined. The gray shading indicates missing data.

3.2. Seasonal Dependence of IOD Prediction Skill

To explore the seasonal dependence of the DMI predictive skill, we assess the ACC (Figure 2) and NRMSE (Figure S6) as a function of lead time and target season. For a better comparison, the differences in ACC and NRMSE among the different models are shown in Figures S7 and S8, respectively. Not surprisingly, SDM-Z exhibits almost the same ACC pattern as the persistence forecast (Figures 2a, 2c, and S7a), as well as a similar NRMSE pattern except at longer lead times (Figures S6a, S6c, and S8a). This confirms that the SDM with seasonally varying damping rate but without forcing can capture the IOD seasonal statistics, very well in agreement with Stuecker et al. (2017). When the seasonal modulated ENSO forcing is included in the SDM, we observe considerable improvements of ACC and NRMSE, especially with a target season in boreal fall at longer lead times (Figures 2e and 2g). The SDM-P provides skillful predictions of the fall DMI with up to three seasons lead time and the SDM-F with up to two seasons lead time.

The SDM-P-F beats CFSv2 with pronounced improved skills in terms of both ACC and NRMSE metrics for target seasons in boreal summer and fall at longer lead times, which are the IOD developing and peak seasons, respectively. Importantly, the SDM-F-F in the operational setting demonstrates significantly improved ACC skill compared to CFSv2 in target season June-July-August at lead times of two to five months. This indicates that the IOD predictive skill in boreal fall and summer could potentially be further improved by improving ENSO predictions.

In contrast to boreal fall and summer, very little predictive skill is evident for the boreal winter target seasons, for which the ACC quickly decreases below 0.4 for a three-month lead time forecast (Figures 2a–2h). This is consistent with the well-known winter prediction barrier for the IOD (Feng et al., 2014; Luo et al., 2007; Wajsowicz, 2007; Zhao & Hendon, 2009), which might be related to the annual reversal of the monsoon (Luo et al., 2007, 2015) and a very small signal to predict for that time of the year (Figure S2b). The prediction barrier for the IOD lasts through the spring and early summer in the persistence and CFSv2 forecasts (Figures 2a and 2b). A recent theoretical study suggests that the IOD prediction barrier is overwhelmingly determined by the seasonal growth rate (Liu et al., 2019). However, this study did not consider the impact of ENSO forcing. Next, we conducted six additional SDM experiments using the same seasonally modulated ENSO forcing but a constant growth rate (see Text S4 and Figures S11 and S12 in the supporting information). The DMI predictive skills in these experiments are very similar to those with seasonal modulated grow rate as shown in Figures 1a, 1b, and 2, suggesting an important influence of ENSO on the IOD prediction barrier. Moreover, the SDM experiments with observed ENSO forcing (SDM-P and SDM-P-F) demonstrate a common feature that the ACC recovers slightly in boreal late winter/early spring (February-March-April) and then decreases again in late spring with minimum ACC values in April-May-June showing a small local peak (Figures 2e and 2f). This rebound is not evident in the SDM without ENSO forcing (Figures 2c and 2d), and only weakly represented in those with CFSv2 forecast ENSO forcing (Figures 2g and 2h), indicating that the IOD spring predictability barrier is related to ENSO (Luo et al., 2015; Wang et al., 2009) and that improved ENSO predictions could also potentially lead to increased IOD predictive skill for a target season in February-March-April.

3.3. Predictability of Individual IOD Events

To investigate the forecast skills for individual IOD events, we compare the time series of the running three-month mean observed DMI with the corresponding model forecasts by SDM-P (which is a measure of the upper IOD predictability limit provided by ENSO), SDM-F-F (the SDM version that can be used in an operational forecast setting), and CFSv2 with start times at zero- to eight-month leads (Figure 3). A further comparison between the models and observations at three- and six-month lead times is shown in Figure S9. For strong IOD events that co-occurred with ENSO events, both the SDM and CFSv2 were able to predict the 1997 positive (occurring during El Niño) and 1998 negative (occurring during La Niña) IOD events with considerable skill more than two seasons before the event (Figure 3). Both CFSv2 and the SDMs underestimate the DMI in the peak season of SON 1997, explaining about 55% of the observed DMI amplitude at three-month lead time. The DMI amplitude during SON 1997 was also underestimated in both SINTEX-F1 and SINTEX-F2 prediction systems (Doi et al., 2017; Luo et al., 2007). In contrast, the DMI amplitude in the peak season of SON 1998 is well captured by the models, attaining over 90% of the observed amplitude in both CFSv2 and SDM-F-F at three- and six-month lead times.

Importantly, CFSv2 completely failed to predict the 2015 positive IOD event, which was predicted one season ahead with the SINTEX-F1 system (Doi et al., 2017). In contrast, the SDM shows enhanced skill and successfully predicts the event two seasons ahead in both the SDM-P and SDM-F-F experiments (Figure 3). The above indicates that the operational dynamical model failed to capture the IOD–ENSO relationship, which then resulted in a DMI prediction failure even when the ENSO state was well predicted (Figure S9). It can be seen in Figure 3 that there are several false alarms in CFSv2 for positive IOD events at six-month lead time such as 2001, 2004, and 2009. These three false alarms are not evident in SDM-P but are weakly represented in SDM-F-F that uses the CFSv2 forecast ENSO forcing. This suggests that warm biases of the predicted N3.4 (Figure S10) may cause false alarms of positive IOD events in CFSv2. In addition, the 2012 positive IOD event was predicted as a negative IOD event in both SINTEX-F1 and SINTEX-F2 (Doi et al., 2016, 2017), and as near-neutral IOD condition in CFSv2. However, it was successfully predicted as a positive IOD with the SDM at one season lead time.

For some strong ENSO-independent IOD events that occurred during neutral ENSO conditions (such as 1994 IOD event) or weak ENSO conditions (such as 2006 IOD event), the predictive skill is limited to a lead time of one season in both CFSv2 and the SDM. The 1994 and 2006 positive IOD events were predicted successfully at lead times of two seasons in both SINTEX-F1 and SINTEX-F2 (Luo et al., 2007; Luo et al., 2008). In addition, many operational prediction systems (CFSv2, SINTEX-F1, and SINTEX-F2; Doi et al., 2017), as well as the SDM, show a false alarm of a negative IOD event during the SON 1988 La Niña developing phase (Figure 3). A recent study (Doi et al., 2017) showed that the 1988 neutral IOD condition was well predicted in the SINTEX-F2 system with three-dimensional observed ocean temperature and salinity information included. This is consistent with previous studies that argue that some potential IOD predictability arises from Indian Ocean subsurface heat content via recharge oscillator dynamics (Feng & Meyers, 2003; McPhaden & Nagura, 2014; Wang et al., 2016). This suggests that subsurface Indian Ocean processes, which are not included in the SDM, may slightly offset the contribution of ENSO to the DMI.

4. Summary and Discussion

In the present study, we developed a simple SDM for predicting the DMI. The SDM without any ENSO forcing demonstrated very similar ACC skills compared to persistence forecast. The SDM with either forecast or perfect ENSO forcing did exhibit higher skill at approximately two- to six-month lead time compared to the operational CFSv2 forecast system. The skillful DMI predictions can be improved up to two seasons of lead time in the SDM with perfect ENSO forcing (SDM-P), which provides a measure of the unutilized skill for IOD forecasts arising from ENSO predictability. When using the SDM in an operational setting by using the forecast ENSO forcing (SDM-F-F), we still achieve an ACC skill increase of 0.1 and above at approximately three- to six-month lead times compared to CFSv2. Concentrating on the DMI averaged for SON and its prediction skill from June initialization in each year, the SDM-F-F performs better than the operational SINTEX-F prediction system. Although there is a large event-to-event skill diversity for the IOD prediction, the superior performance of the SDM is evident for most IOD events. We also showed that operational IOD predictability beyond persistence is mostly attributable to ENSO predictability and influenced by the signal-to-noise ratio of the system.

The present results provide a novel perspective for improving our ability to predict the IOD. Our results demonstrate that operational predictions of ENSO should translate into better future predictions of the IOD if we utilize the SDM. Importantly, we should be able to further improve IOD predictability by improving ENSO predictions in the current generation of operational forecast models. We hypothesize that additional improvements in IOD prediction skill could be achieved in coupled general circulation models and the SDM, for instance, by improved data assimilation, more realistic ENSO atmospheric teleconnections, and better representations of Indian Ocean intrinsic dynamics (Crétat et al., 2017; Doi et al., 2017). For instance, including Indian Ocean subsurface heat content information as an additional predictor in the SDM could lead to improvements in the prediction skill of ENSO-independent IOD events via recharge oscillator dynamics (McPhaden & Nagura, 2014). Additionally, given that the IOD–ENSO relationship varies for different ENSO types (Zhang et al., 2015), considering different ENSO flavors in the SDM forcing might lead to further improvement in the prediction of ENSO-dependent IOD events.

Acknowledgments
This research was supported by the U.S. National Science Foundation (AGS-1406601 and AGS-1813611) and U.S. Department of Energy (DESC005110). M.F.S. was supported by the Institute for Basic Science (project code IBS-R028-D1). We thank M. Hayashi for the critical reading of the manuscript and four anonymous reviewers for their constructive comments. The CFSv2 retrospective and real-time forecasts are publicly available and can be downloaded from http://iridl.ldeo.columbia.edu/. The NOAA OISST V2 data are publicly available at http://www.esrl.noaa.gov/psd/data/gridded/data.noaa.oisst.v2.html. The ERA-Interim reanalysis data are available at http://apps.ecmwf.int/datasets/. The SDM hindcasts and the data that support the findings of this study are publicly available at https://doi.org/10.5281/zenodo.3251130.

References

Annamalai, H., Murtugudde, R., Potemra, J., & Xie, S. P. (2003). Coupled dynamics over the Indian Ocean: Spring initiation of the zonal mode. *Deep-Sea Research Part II*, *50*(12–13), 2305–2330. https://doi.org/10.1016/s0967-0645(03)00058-4

Barnston, A. G., Tippett, M. K., L'Heureux, M. L., Li, S., & DeWitt, D. G. (2012). Skill of real-time seasonal ENSO model predictions during 2002–11: Is our capability increasing? *Bulletin of the American Meteorological Society*, *93*(5), 631–651. https://doi.org/10.1175/BAMS-D-11-00111.1

Barnston, A. G., Tippett, M. K., L'Heureux, M. L., & Ranganathan, M. (2017). Deterministic skill of ENSO predictions from the North American Multimodel Ensemble. *Climate Dynamics*, 1–20. https://doi.org/10.1007/s00382-017-3603-3

Behera, S. K., Luo, J.-J., Masson, S., Rao, S. A., Sakuma, H., & Yamagata, T. (2006). A CGCM Study on the Interaction between IOD and ENSO. *Journal of Climate*, *19*(9), 1688–1705. https://doi.org/10.1175/JCLI3797.1

Behera, S. K., & Yamagata, T. (2003). Influence of the Indian Ocean Dipole on the Southern Oscillation. *Journal of the Meteorological Society Japan*, *81*(1), 169–177. https://doi.org/10.2151/jmsj.81.169

Cai, W., & Qiu, Y. (2013). An observation-based assessment of nonlinear feedback processes associated with the Indian Ocean Dipole. *Journal of Climate*, *26*(9), 2880–2890. https://doi.org/10.1175/JCLI-D-12-00483.1

Cai, W., Santoso, A., Wang, G., Weller, E., Wu, L., Ashok, K., et al. (2014). Increased frequency of extreme Indian Ocean Dipole events due to greenhouse warming. *Nature*, *510*(7504), 254–258. https://doi.org/10.1038/nature13327

Cai, W., van Rensch, P., Cowan, T., & Hendon, H. H. (2011). Teleconnection pathways of ENSO and the IOD and the mechanisms for impacts on Australian rainfall. *Journal of Climate*, *24*(15), 3910–3923. https://doi.org/10.1175/2011jcli4129.1

Chan, S. C., Behera, S. K., & Yamagata, T. (2008). Indian Ocean Dipole influence on South American rainfall. *Geophysical Research Letters*, *35*, L14s12. https://doi.org/10.1029/2008GL034204

Crétat, J., Terray, P., Masson, S., & Sooraj, K. P. (2017). Intrinsic precursors and timescale of the tropical Indian Ocean Dipole: Insights from partially decoupled numerical experiment. *Climate Dynamics*, *51*(4), 1311–1332. https://doi.org/10.1007/s00382-017-3956-7

De Elvira, A. R., & Lemke, P. (1982). A Langevin equation for stochastic climate models with periodic feedback and forcing variance. *Tellus*, *34*(4), 313–320. https://doi.org/10.1111/j.2153-3490.1982.tb01821.x

Doi, T., Behera, S. K., & Yamagata, T. (2016). Improved seasonal prediction using the SINTEX-F2 coupled model. *Journal of Advances in Modeling Earth Systems*, *8*, 1847–1867. https://doi.org/10.1002/2016MS000744

Doi, T., Storto, A., Behera, S. K., Navarra, A., & Yamagata, T. (2017). Improved prediction of the Indian Ocean Dipole mode by use of subsurface ocean observations. *Journal of Climate*, *30*(19), 7953–7970. https://doi.org/10.1175/JCLI-D-16-0915.1

Dommenget, D., & Jansen, M. (2009). Predictions of Indian Ocean SST indices with a simple statistical model: A null hypothesis. *Journal of Climate*, *22*(18), 4930–4938. https://doi.org/10.1175/2009JCLI2846.1

Feng, M., & Meyers, G. (2003). Interannual variability in the tropical Indian Ocean: A two-year time-scale of Indian Ocean Dipole. *Deep-Sea Research Part II*, *50*(12-13), 2263–2284. https://doi.org/10.1016/S0967-0645(03)00056-0

Feng, R., Duan, W., & Mu, M. (2014). The "winter predictability barrier" for IOD events and its error growth dynamics: Results from a fully coupled GCM. *Journal of Geophysical Research: Oceans*, *119*, 8688–8708. https://doi.org/10.1002/2014JC010473

Fischer, A. S., Terray, P., Guilyardi, E., Gualdi, S., & Delecluse, P. (2005). Two independent triggers for the Indian Ocean Dipole/zonal mode in a coupled GCM. *Journal of Climate*, *18*(17), 3428–3449. https://doi.org/10.1175/JCLI3478.1

Frankignoul, C., & Hasselmann, K. (1977). Stochastic climate models: Part II—Application to sea-surface temperature anomalies and thermocline variability. *Tellus*, *29*(4), 289–305. https://doi.org/10.1111/j.2153-3490.1977.tb00740.x

Guan, Z. Y., & Yamagata, T. (2003). The unusual summer of 1994 in East Asia: IOD teleconnections. *Geophysical Research Letters*, *30*(10), 1544. https://doi.org/10.1029/2002GL016831

Hasselmann, K. (1976). Stochastic climate models: Part I. Theory. *Tellus*, *28*(6), 473–485. https://doi.org/10.1111/j.2153-3490.1976.tb00696.x

Hong, C.-C., Li, T., Ho, L., & Kug, J.-S. (2008). Asymmetry of the Indian Ocean Dipole. Part I: Observational analysis. *Journal of Climate*, *21*(18), 4834–4848. https://doi.org/10.1175/2008JCLI2222.1

Izumo, T., Vialard, J., Lengaigne, M., de Boyer Montegut, C., Behera, S. K., Luo, J., et al. (2010). Influence of the state of the Indian Ocean dipole on the following year's El Niño. *Nature Geoscience*, *3*(3), 168–172. https://doi.org/10.1038/ngeo760

Jin, F.-F., Lin, L., Timmermann, A., & Zhao, J. (2007). Ensemble-mean dynamics of the ENSO recharge oscillator under state-dependent stochastic forcing. *Geophysical Research Letters*, *34*, L03807. https://doi.org/10.1029/2006GL027372

Kajtar, J. B., Santoso, A., England, M. H., & Cai, W. (2017). Tropical climate variability: Interactions across the Pacific, Indian, and Atlantic Oceans. *Climate Dynamics*, *48*(7–8), 2173–2190. https://doi.org/10.1007/s00382-016-3199-z

Li, T., Wang, B., Chang, C.-P., & Zhang, Y. (2003). A theory for the Indian Ocean Dipole–Zonal Mode. *Journal of the Atmospheric Sciences*, *60*(17), 2119–2135. https://doi.org/10.1175/1520-0469(2003)060<2119:ATFTIO>2.0.CO;2

Liu, H., Tang, Y., Chen, D., & Lian, T. (2017). Predictability of the Indian Ocean Dipole in the coupled models. *Climate Dynamics*, *48*(5–6), 2005–2024. https://doi.org/10.1007/s00382-016-3187-3

Liu, N., Chen, H. X., & Lu, L. G. (2007). Teleconnection of IOD signal in the upper troposphere over southern high latitudes. *Journal of Oceanography*, *63*(1), 155–157. https://doi.org/10.1007/s10872-007-0014-9

Liu, Z., Jin, Y., & Rong, X. (2019). A theory for the seasonal predictability barrier: Threshold, timing, and intensity. *Journal of Climate*, *32*(2), 423–443. https://doi.org/10.1175/JCLI-D-18-0383.1

Loschnigg, J., Meehl, G. A., Webster, P. J., Arblaster, J. M., & Compo, G. P. (2003). The Asian monsoon, the tropospheric biennial oscillation, and the Indian Ocean Zonal Mode in the NCAR CSM*. *Journal of Climate*, *16*(11), 1617–1642. https://doi.org/10.1175/1520-0442(2003)016<1617:TAMTTB>2.0.CO;2

Luo, J.-J., Behera, S. K., Masumoto, Y., Sakuma, H., & Yamagata, T. (2008). Successful prediction of the consecutive IOD in 2006 and 2007. *Geophysical Research Letters*, *35*, L14S02. https://doi.org/10.1029/2007GL032793

Luo, J.-J., Masson, S., Behera, S. K., & Yamagata, T. (2007). Experimental forecasts of the Indian Ocean Dipole using a coupled OAGCM. *Journal of Climate*, *20*(10), 2178–2190. https://doi.org/10.1175/JCLI4132.1

Luo, J.-J., Yuan, C., Sasaki, W., Behera, S. K., Masumoto, Y., Yamagata, T., et al. (2015). Current status of intraseasonal–seasonal-to-interannual prediction of the Indo-Pacific climate. In S. K. Behera, & T. Yamagata (Eds.), *Indo-Pacific climate variability and predictability*, World Scientific Series on Asia-Pacific Weather and Climate (pp. 63–107). Singapore: World Scientific. https://doi.org/10.1142/9789814696623_0003

Luo, J.-J., Zhang, R., Behera, S. K., Masumoto, Y., Jin, F.-F., Lukas, R., & Yamagata, T. (2010). Interaction between El Niño and extreme Indian Ocean Dipole. *Journal of Climate*, *23*(3), 726–742. https://doi.org/10.1175/2009JCLI3104.1

McPhaden, M. J., & Nagura, M. (2014). Indian Ocean dipole interpreted in terms of recharge oscillator theory. *Climate Dynamics*, *42*(5–6), 1569–1586. https://doi.org/10.1007/s00382-013-1765-1

Moon, W., & Wettlaufer, J. S. (2017). A unified nonlinear stochastic time series analysis for climate science. *Scientific Reports*, *7*(1), 44228. https://doi.org/10.1038/srep44228

Ng, B., Cai, W., & Walsh, K. (2014). The role of the SST-thermocline relationship in Indian Ocean Dipole skewness and its response to global warming. *Scientific Reports*, *4*(1), 6034. https://doi.org/10.1038/srep06034

Reynolds, R. W., Rayner, N. A., Smith, T. M., Stokes, D. C., & Wang, W. (2002). An improved in situ and satellite SST analysis for climate. *Journal of Climate*, *15*(13), 1609–1625. https://doi.org/10.1175/1520-0442(2002)015<1609:AIISAS>2.0.CO;2

Saha, S., Moorthi, S., Wu, X., Wang, J., Nadiga, S., Tripp, P., et al. (2014). The NCEP Climate Forecast System version 2. *Journal of Climate*, *27*(6), 2185–2208. https://doi.org/10.1175/JCLI-D-12-00823.1

Saji, N. H., Goswami, B. N., Vinayachandran, P. N., & Yamagata, T. (1999). A dipole mode in the tropical Indian Ocean. *Nature*, *401*(6751), 360–363. https://doi.org/10.1038/43855

Saji, N. H., Xie, S. P., & Yamagata, T. (2006). Tropical Indian Ocean variability in the IPCC twentieth-century climate simulations. *Journal of Climate*, *19*(17), 4397–4417. https://doi.org/10.1175/JCLI3847.1

Saji, N. H., & Yamagata, T. (2003a). Structure of SST and surface wind variability during Indian ocean dipole mode events: COADS observations. *Journal of Climate*, *16*(16), 2735–2751. https://doi.org/10.1175/1520-0442(2003)016<2735:Sosasw>2.0.Co;2

Saji, N. H., & Yamagata, T. (2003b). Possible impacts of Indian Ocean Dipole mode events on global climate. *Climate Research*, *25*(2), 151–169. https://doi.org/10.3354/cr025151

Shi, L., Hendon, H. H., Alves, O., Luo, J.-J., Balmaseda, M., & Anderson, D. (2012). How predictable is the Indian Ocean Dipole? *Monthly Weather Review*, *140*(12), 3867–3884. https://doi.org/10.1175/MWR-D-12-00001.1

Song, Q., Vecchi, G. A., & Rosati, A. J. (2008). Predictability of the Indian Ocean sea surface temperature anomalies in the GFDL coupled model. *Geophysical Research Letters*, *35*, L02701. https://doi.org/10.1029/2007GL031966

Stuecker, M. F., Jin, F.-F., Timmermann, A., & McGregor, S. (2015). Combination mode dynamics of the anomalous Northwest Pacific anticyclone. *Journal of Climate*, *28*(3), 1093–1111. https://doi.org/10.1175/JCLI-D-14-00225.1

Stuecker, M. F., Timmermann, A., Jin, F.-F., Chikamoto, Y., Zhang, W., Wittenberg, A. T., et al. (2017). Revisiting ENSO/Indian Ocean Dipole phase relationships. *Geophysical Research Letters*, *44*, 2481–2492. https://doi.org/10.1002/2016GL072308

Stuecker, M. F., Timmermann, A., Jin, F.-F., McGregor, S., & Ren, H.-L. (2013). A combination mode of the annual cycle and the El Niño/Southern Oscillation. *Nature Geoscience*, *6*(7), 540–544. https://doi.org/10.1038/ngeo1826

Wajsowicz, R. C. (2005). Potential predictability of tropical Indian Ocean SST anomalies. *Geophysical Research Letters*, *32*, L24702. https://doi.org/10.1029/2005GL024169

Wajsowicz, R. C. (2007). Seasonal-to-interannual forecasting of tropical Indian Ocean sea surface temperature anomalies: Potential predictability and barriers. *Journal of Climate*, *20*(13), 3320–3343. https://doi.org/10.1175/jcli4162.1

Wang, B., Lee, J.-Y., Kang, I.-S., Shukla, J., Park, C. K., Kumar, A., et al. (2009). Advance and prospectus of seasonal prediction: assessment of the APCC/CliPAS 14-model ensemble retrospective seasonal prediction (1980–2004). *Climate Dynamics*, *33*(1), 93–117. https://doi.org/10.1007/s00382-008-0460-0

Wang, H., Kumar, A., Murtugudde, R., Narapusetty, B., & Seip, K. L. (2019). Covariations between the Indian Ocean dipole and ENSO: A modeling study. *Climate Dynamics*, 1–19. https://doi.org/10.1007/s00382-019-04895-x

Wang, H., Murtugudde, R., & Kumar, A. (2016). Evolution of Indian Ocean dipole and its forcing mechanisms in the absence of ENSO. *Climate Dynamics*, *47*(7-8), 2481–2500. https://doi.org/10.1007/s00382-016-2977-y

Webster, P. J., Moore, A. M., Loschnigg, J. P., & Leben, R. R. (1999). Coupled ocean–atmosphere dynamics in the Indian Ocean during 1997–98. *Nature*, *401*(6751), 356–360. https://doi.org/10.1038/43848

Xie, S.-P., & Zhou, Z.-Q. (2017). Seasonal modulations of El Niño-related atmospheric variability: Indo–Western Pacific Ocean feedback. *Journal of Climate*, *30*(9), 3461–3472. https://doi.org/10.1175/JCLI-D-16-0713.1

Yang, Y., Xie, S.-P., Wu, L., Kosaka, Y., Lau, N.-C., & Vecchi, G. A. (2015). Seasonality and predictability of the Indian Ocean Dipole mode: ENSO forcing and internal variability. *Journal of Climate*, *28*(20), 8021–8036. https://doi.org/10.1175/JCLI-D-15-0078.1

Yuan, Y., Yang, H., Zhou, W., & Li, C. Y. (2008). Influences of the Indian Ocean dipole on the Asian summer monsoon in the following year. *International Journal of Climatology*, *28*(14), 1849–1859. https://doi.org/10.1002/joc.1678

Zhang, W., Wang, Y., Jin, F.-F., Stuecker, M. F., & Turner, A. G. (2015). Impact of different El Niño types on the El Niño/IOD relationship. *Geophysical Research Letters*, *42*, 8570–8576. https://doi.org/10.1002/2015GL065703

Zhao, M., & Hendon, H. H. (2009). Representation and prediction of the Indian Ocean dipole in the POAMA seasonal forecast model. *Quarterly Journal of the Royal Meteorological Society*, *135*(639), 337–352. https://doi.org/10.1002/qj.370

Zhu, J., Huang, B., Kumar, A., & Kinter, J. L. III (2015). Seasonality in prediction skill and predictable pattern of tropical Indian Ocean SST. *Journal of Climate*, *28*(20), 7962–7984. https://doi.org/10.1175/JCLI-D-15-0067.1